

Simulations and experimental validation of lightning-induced voltages on a PV system in both common mode and differential mode

Simisi Mosamane^{*}, Chandima Gomes

University of the Witwatersrand, Johannesburg, South Africa

ARTICLE INFO

Keywords:

Impulse current
Lightning-induced overvoltages
Microinverters
Lightning protection
PV systems

ABSTRACT

Lightning-induced overvoltages (LIOs) can destroy, degrade, or cause malfunctions in photovoltaic installations (PVIs). Therefore, this overvoltage risk necessitates the protection of PVIs. In the last few years, microinverters have increased the market segmentation in small and medium-sized photovoltaic (PV) systems. These devices have lower voltage and current ratings than central or string inverters; therefore, they are more sensitive to lightning stresses. In the present study, which precedes lightning protection evaluations for microinverters, lightning-induced overvoltage simulations, performed using COMSOL Multiphysics® software and validated experimentally, indicate the influence of electromagnetic coupling on PV systems caused by lightning transients. The results suggest that the induced overvoltages measured on DC cables during lightning strikes vary for different protection scenarios and current magnitudes. The common-mode (CM) induced voltages were significantly greater than the differential-mode (DM) induced voltages. The induced voltages exhibited a further linear increase with the magnitude of the impulse current. Furthermore, the induced voltages measured as the impulse current was injected into the PV system's frame were higher than when the impulse current was injected into the lightning protection system (LPS) structure. The understanding of the differences in these voltages and the parameters of influence is crucial for protection engineers when selecting SPDs for PV installations with microinverters.

1. Introduction

Microinverter applications and designs, in line with the inversion process, have been topics of interest for the design of photovoltaic (PV) systems [1]. However, overvoltage has been identified as one of the top five risks of microinverter failure, which may affect these components before their expected lifespan of 25 years [2,3]. Lightning transients and their subsequent induced overvoltages can have adverse effects on equipment and structures, including failure of electronic equipment. In an electrical network, a phase conductor is susceptible to being directly struck by lightning, allowing the overvoltage to propagate through the conductor and damage the connected electrical equipment. An indirect lightning strike can occur in two ways: through a ground current when lightning strikes the ground and travels until it reaches an object, or as a side flash passing through the air to a second object [4,5]. This phenomenon was first explained by the bound charge theory, which was accepted in the 20th century for lightning-induced overvoltage. The latest theories explain this process: the lightning channel between clouds and the ground contains a subsequent return stroke, during

which the radiated electromagnetic fields induce overvoltage [4,6].

The lightning current parameters, which are essential for developing protection measures, have been widely studied in lightning research [7, 8]. The lightning return stroke current has a relatively high peak, followed by slow decay [7]. The time taken from zero to achieve the peak value is defined as the front time, and the subsequent decay time is called tail time. Each of these parameters is important for the design of protection systems. However, in an earthing system, the highest value of stroke, maximum peak current, and the total charge for the melting points of the attachment are crucial. Furthermore, the specific flash energy is responsible for the mechanical forces. Finally, the maximum rate of rise is also responsible for the maximum induced voltage of electronics [9].

Evaluations of lightning-induced overvoltages (LIOs) are essential for designing and coordinating protection measures for electrical systems (Table 1). These studies, which have been conducted on modules and strings, have shown that the voltages induced by nearby lightning transients are caused by the internal loop created by the interconnection of the cells and metal frame of the PV module. The magnitudes and

^{*} Corresponding author.

E-mail address: simisi.mosamane@gmail.com (S. Mosamane).

Table 1
Lightning induced voltages studies for PV systems.

Ref	Methods	Contribution	Lightning Current Amplitude	LPS/ lightning striking distance	Soil resistivity	Common Mode/ Differential Mode	Cable Length
[10]	Experiment	Used a highspeed datalogger to perform voltage measurements between the terminals of the two photovoltaic arrays to measure the lightning-induced overvoltage.		x			
[12]	Experiment Simulation	Using a modified mesh current method, measured induced voltages for different case studies	x	x	x		
[13]	Experiment Simulation	Measured induced voltages on long DC cabling loops on a PV system		x			
[14]	Experiment	Used a software tool to measure induced currents and voltages on PV systems					
[15]	Simulation	Using a simulation tool, measured induced overvoltages and currents based on striking locations	x	x			x
[16]	Experiment	Measured the variation of induced voltages when lightning strikes at different positions		x			
[17]	Simulation	Analysed induced voltages in CM and DM using a semi-analytical 3D numerical model				x	
[18]	Simulation	Measured induced voltages on a hybrid PV-energy storage system	x	x			x
[11]	Simulation	Measured induced voltages for PV panels installed on a mountain		x			
[6]	Simulation	Measured induced voltages using a PEEC method on a PV systems		x			

waveforms of these voltages can be used to develop, design, or select surge protection for PV systems. Several studies have concluded that lightning striking closer to a panel may be destructive to inverters because of the high voltages associated with lightning surges [6,10–12]. Most studies in this area have focused on Differential Mode (DM) measurements. However, common-mode (CM)-induced voltage effects have not been studied extensively. Additionally, most current studies were concerned with central and sometimes string inverters; but there is minimal information about the protection of microinverters in previous studies.

In this study, we investigated the induced voltages using COMSOL Multiphysics® simulation software with two simulated current waveforms (10/350 μ s and 8/20 μ s using the Heidler function) injected in different protection scenarios at various impulse current magnitudes. The lowest impulse current magnitude adopted in the simulation was 5 kA, and the highest was 100 kA. Despite the low probability of occurrence, the highest impulse current was favourable for the most severe circumstances. This study was further validated through experiments with impulse currents not exceeding 20 kA [19].

1.1. Coupling models

The evaluation of light-induced voltages is typically conducted using the following steps [20].

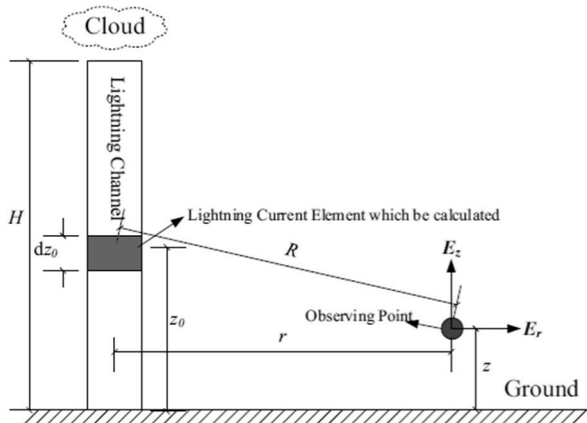


Fig. 1. Electromagnetic propagation model of return stroke.

- The lightning return-stroke current model, as a function of time and height, is employed at several points by considering the lightning return-stroke electromagnetic field change.
- A selected coupling model is then used to calculate the lightning-induced voltages based on the interaction between the line conductors and the field.

LIOs are composed of electrostatic and electromagnetic components, namely horizontal and vertical components [4]. The electromagnetic propagation model, as shown in Fig. 1 [21], can be described using the vertical electric field (E_z), the horizontal electric field (E_r), and the horizontal magnetic field (H_r):

$$E_z(r, z, t) = \frac{1}{4\pi\epsilon_0} \left(\int_{-H}^H \frac{2(z-z_0)^2 - r^2}{R^5} \int_0^t i\left(z_0, \tau - \frac{R}{c}\right) d\tau dz_0 + \int_{-H}^H \frac{2(z-z_0)^2 - r^2}{cR^4} i\left(z_0, t - \frac{R}{c}\right) dz_0 - \int_{-H}^H \frac{r^2}{c^2 R^2} \frac{\partial i\left(z_0, t - \frac{R}{c}\right)}{\partial t} dz_0 \right) \quad (1)$$

$$E_r(r, z, t) = \frac{1}{4\pi\epsilon_0} \left(\int_{-H}^H \frac{3r(z-z_0)}{R^5} \int_0^t i\left(z_0, \tau - \frac{R}{c}\right) d\tau dz_0 + \int_{-H}^H \frac{3r(z-z_0)^2 - r^2}{cR^4} i\left(z_0, t - \frac{R}{c}\right) dz_0 - \int_{-H}^H \frac{r(z-z_0)}{c^2 R^2} \frac{\partial i\left(z_0, t - \frac{R}{c}\right)}{\partial t} dz_0 \right) \quad (2)$$

$$E_r(r, z, t) = H_r(r, z, t) \frac{1}{4\pi} \left(\int_{-H}^H \frac{r}{R^2} i \left(z_0, t - \frac{R}{c} \right) dz_0 + \int_{-H}^H \frac{r}{cR^2} \frac{\partial i \left(z_0, t - \frac{R}{c} \right)}{\partial t} dz_0 \right) \quad (3)$$

where r is the distance from the observation point to the leader channel; z_0 is the height of the object being calculated; τ is the integration time variable; and R is the distance between the calculation and observation points.

The simulations of electromagnetic transients are extremely popular. Models performing these calculations have been developed, including the Rusck, Chowdry, and Agrawal models. These models mainly focused on the physical processes of the return stroke.

The Rusck [22] model can be expressed as:

$$\frac{\partial \varnothing(x, t)}{\partial x} + L' \frac{\partial i(x, t)}{\partial t} = 0 \quad (4)$$

$$\frac{\partial i(x, t)}{\partial x} + C' \frac{\partial}{\partial t} [\varnothing(x, t) - \varnothing^i(x, t)] = 0 \quad (5)$$

where C' and L' are the line capacitance and inductance per unit length, respectively and \varnothing is the induced scalar potential.

The total induced voltage can be expressed as:

$$v(x, t) = \varnothing(x, t) + \int_0^h \frac{\partial A_z^e(x, z, t)}{\partial t} dz \quad (6)$$

where A_z^e is the vertical component of the incident vector potential, and h is the conductor height.

The equations describing the transmission line coupling using the Agrawal model [23] are expressed as:

$$\frac{\partial}{\partial x} [u_i^s(x, t)] + [R'_{ij}] \cdot i_i(x, t) + [L'_{ij}] \cdot \frac{\partial}{\partial t} [i_i(x, t)] = [E_x^i(x, h_i, t)] \quad (7)$$

$$\frac{\partial}{\partial x} [i_i(x, t)] + [G'_{ij}] \cdot u_i^s(x, t) + [C'_{ij}] \cdot \frac{\partial}{\partial t} [u_i^s(x, t)] = 0 \quad (8)$$

$[E_x^i(x, h_i, t)]$ is the vector of the horizontal component of the incident electric field along the x axis at conductor height h_i , $[L'_{ij}]$, $[R'_{ij}]$, $[C'_{ij}]$, $[G'_{ij}]$ are the inductance, resistance, capacitance, and conductance matrices, respectively.

The total line voltage $[u_i(x, t)]$ can be expressed as:

$$u_i(x, t) = u_i^s(x, t) + u_i^i(x, t) = u_i^s(x, t) - \left[\int_0^{h_i} E_z^i(x, z, t) dz \right] \quad (9)$$

where $E_z^i(x, z, t)$ is the incident (or inducing) vertical electric field.

The Chowdry-Gross model [24] which has also been used in lightning literature, can be expressed as [25]:

$$\frac{\partial u(x, t)}{\partial x} + L' \frac{\partial i(x, t)}{\partial t} = 0 \quad (10)$$

$$\frac{\partial i(x, t)}{\partial x} + C' \frac{\partial}{\partial t} [u(x, t) - u_i(x, t)] = 0 \quad (11)$$

where the induced voltage $u_i(x, t)$ is expressed as:

$$u_i(x, t) = \int_0^{h_i} E_z^i(x, z, t) dz$$

2. Methodology

2.1. Case studies

COMSOL Multiphysics® simulation software was used for the simulation, which can solve electromagnetic problems by coupling several physical problems in three dimensions, and the components can be assigned material properties. The simulation process is illustrated in Fig. 2. The case studies were as follows:

- Case Study 1:** In this case study, an impulse current was injected into the external lightning protection system (LPS) at distances of 1, 2, and 3 m from the PV panel). The induced voltages were measured across the DC cables in the Differential Mode (DM) and Common Mode (CM) configurations.
- Case Study 2:** The second case study represents a scenario without a lightning protection system. An impulse current was injected into the frame of the PV system, and the resulting induced voltages were measured between the DC cables.

In addition, the influence of wire length was investigated using cable lengths of 1, 2, and 3 m for both case studies.

2.1.1. Modelling of the components

The panel components, including the aluminium frame, tempered glass, ethylene vinyl acetate (film) (EVA), back sheet, and DC cables,

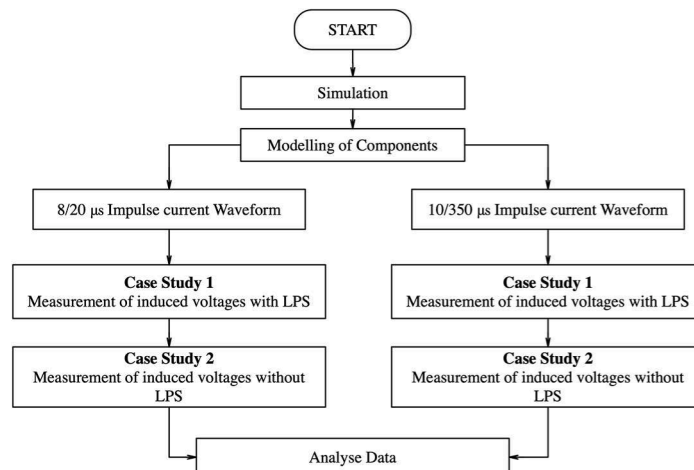


Fig. 2. COMSOL Multiphysics® simulation process flow.

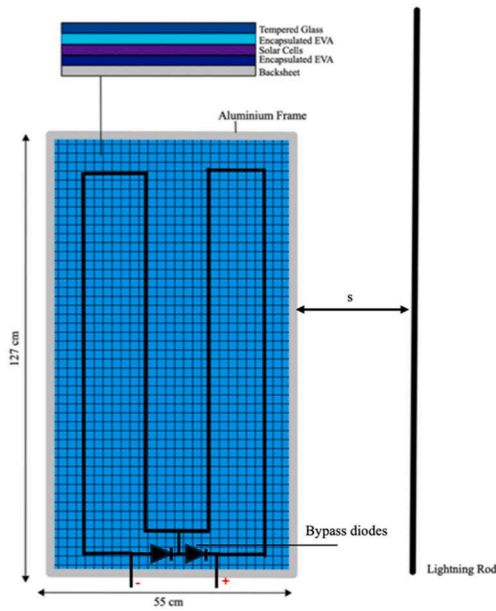


Fig. 3. PV Panel and lightning rod.

Table 2
Material properties.

Material	Relative Permeability (μ_r)	Relative Permittivity (ϵ_r)	Electrical Conductivity (S/m)
Steel	750	1	4.032×10^6
Aluminium	1	1	3.77×10^7
Air	1	1	3×10^{-15}
Glass	1	4.2	1×10^{-14}
Copper	1	1	5.99×10^7
Silicon	1	11.68	1.56×10^{-3}
Ethylene Vinyl Acetate	1	1	3.45×10^{-9}

were modelled to represent the PV panel (Fig. 3). All materials were built in three dimensions in COMSOL and assigned with material properties, as shown in Table 2. For measuring lightning induced overvoltages, the correct modelling of the equipment was crucial, as the slightest errors in the measurements and parameters can significantly influence the results. A voltage-measuring device was then connected between the DC cables to measure the overvoltages induced by lightning currents. Finally, using the software’s capabilities, the electrical circuit

(AC/DC) module was coupled with the magnetic field module to provide an interaction between the circuit and electromagnetic fields for performing calculations using Maxwell’s equations at the macroscopic level under boundary conditions. Figs. 4 and 5 illustrate the designs of Case Studies 1 and 2, respectively.

2.1.2. Modelling of lightning currents

A lightning stroke was simulated as a current source. To generate high impulse currents, the Heidler function, which has been used extensively in lightning research, was used as an analytical function in COMSOL Multiphysics® for two current waveforms (8/20 μ s and 10/350 μ s). Impulse currents of 8/20 μ s and 10/350 μ s, represented by the Heidler function specified by IEC 62,305-1:2010 [26] with peak currents of 5, 12.5, 20, and 100 kA, were simulated.

The Heidler function, presently the standard for the current model, is expressed by the following equation [27]:

$$i(t) = \frac{i_0}{\eta} \frac{\left(\frac{t}{\tau_1}\right)^n}{1 + \left(\frac{t}{\tau_1}\right)^n} \exp\left(-\frac{t}{\tau_2}\right) \tag{12}$$

where i_0 is the peak current, η is the peak current correction, τ_1 is the rise time constant, τ_2 is the decay time constant, and n is the steepness factor.

From Eq. (12), the peak current correction can be expressed as:

$$\eta = \exp\left[\frac{-\tau_1}{\tau_2 \left(\frac{n\tau_2}{\tau_1}\right)^{\frac{1}{n+1}}} \right] \tag{13}$$

The simulated lightning currents for 8/20 μ s and 10/350 μ s standard lightning waveforms are shown in Fig. 6(a) and (b), respectively.

2.2. Experimental investigation

A laboratory experiment was conducted at the High Voltage Laboratory at the University of Witwatersrand. The experimental study, performed under different case studies, aimed to determine the electromagnetic influence of lightning on PV systems within the vicinity of the lightning strike and was used as a primary validation method.

2.2.1. Generation of high impulse current

In alignment with the simulation studies, our experimental enquiry employed both the 8/20 μ s and 10/350 μ s impulse current generators. Circuit parameters of the impulse generator were meticulously adjusted

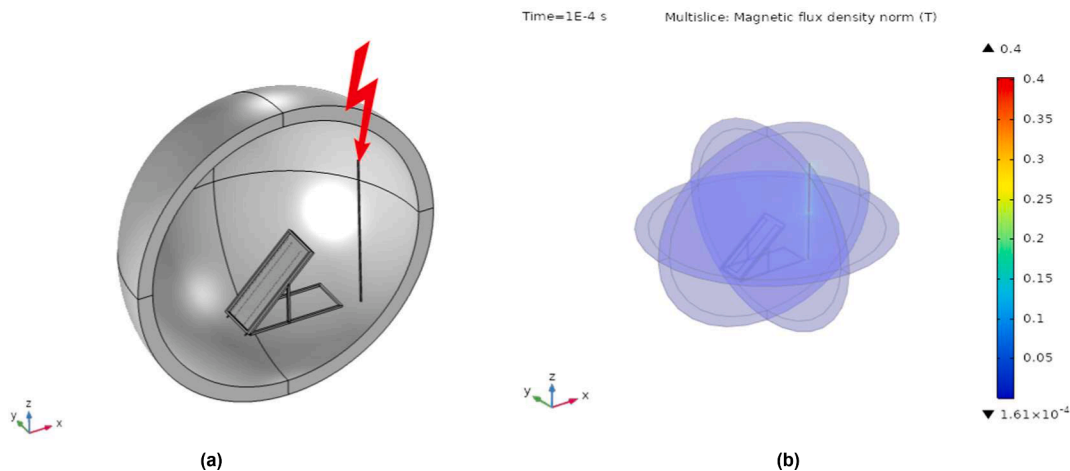


Fig. 4. (a) Case study 1: COMSOL Multiphysics® simulation software setup. (a) Pre-computation (b) After computation.

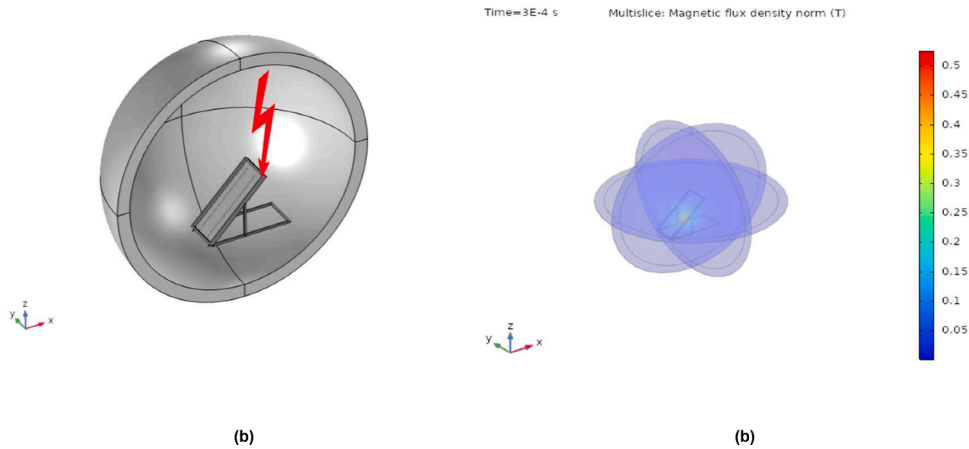


Fig. 5. (a) Case study 2: COMSOL Multiphysics® simulation software setup. (a) Pre-computation (b) After computation.

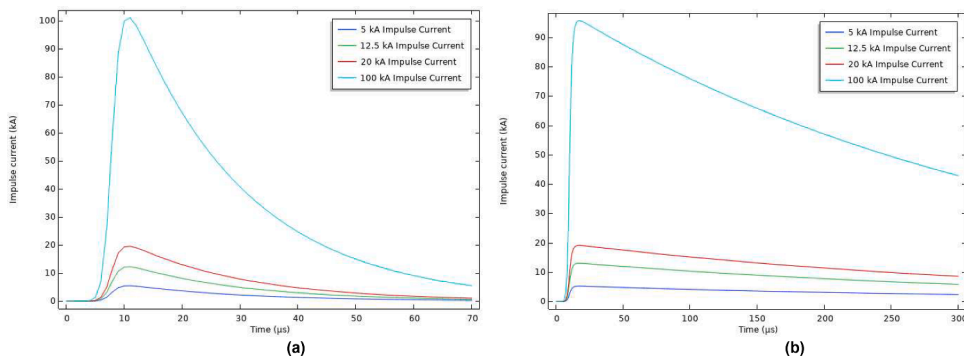


Fig. 6. Simulated 8/20 μs standard surge current waveform. (b) Simulated 10/350 μs standard lightning current waveform.

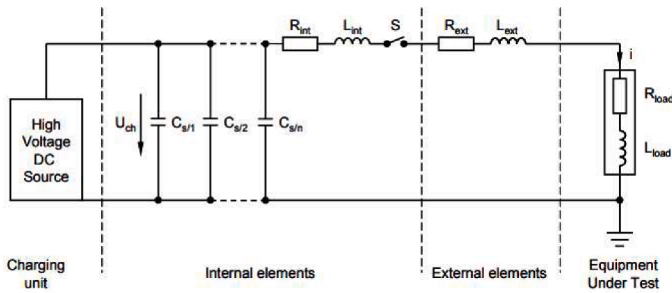


Fig. 7. 10/350 μs High current impulse generator.

to achieve the desired shape of the impulse current. These generators-maintained tolerances of $\pm 10\%$ for peak values and $\pm 20\%$ for fall times. Fig. 7 presents the circuit diagram of the high impulse current generator, composed of a DC charging set with non-inductive charging resistors, charging and discharging capacitors, waveshaping resistors and capacitors, and the triggering system.

2.2.2. Voltage and current measurement

The impulse current was measured using a Pearson Electronics coil (current transformer). The output received from the oscilloscope is a voltage proportional to the current on the device, this value being 0.01 V for 1 A. The protection circuit was connected to the oscilloscope via a coaxial cable. The differential voltage across the shunt resistor was measured by the oscilloscope. The induced voltages on the PV system were measured using an oscilloscope triggered to measure the rising edge of the voltage waveform. Fig. 8

3. Results and discussions

3.1. Case study 1

In this study, we observed that the maximum induced overvoltage depended on the distance between the LPS and the PV panels. Fig 9(a) shows the DM voltage waveforms when the LPS was 1 m, 2 m, and 3 m from the panel under 8/20 μs and 10/350 μs impulse current waveforms at 100-kA impulse current. This is the transient voltage transmitted to the microinverter during the lightning strike. From this observation, when a 100-kA impulse current was injected into the external LPS one metre from the panel, the overvoltage measured on the DC cables in the DM configuration under an 8/20 μs waveform was 2.31 kV. For the 10/350 μs impulse waveform, the maximum induced voltage was 2.2 kV at a 100-kA impulse current.

When the same impulse current was injected 2 m from the panel, induced overvoltages of 837 V and 812 V were observed for the 8/20 μs and 10/350 μs impulse current waveforms in the DM configuration. A further increase to 3 m in the LPS-PV panel distance indicated a further reduction in overvoltages of 384.9 V and 376 V for the 8/20 μs 10/350 μs impulse currents, respectively. The resulting overvoltages for the various impulse currents are listed in Table 3. Generally, PV installations consist of multiple panels coupled to an array. These results demonstrate that nearby lightning strikes may affect the other PV panels within the PV system. The incremental increase in the distance between the PV panel and LPS indicates a reduction in the induced overvoltages. A higher magnetic intensity may arise when the LPS is closer to the panel due to lightning current. This further results in a higher magnetic flux passing across the internal loop and, therefore, greater induced voltages. This observation indicates that the distance from the panel is crucial for the induced voltages measured across the DC cables of the PV panel. In

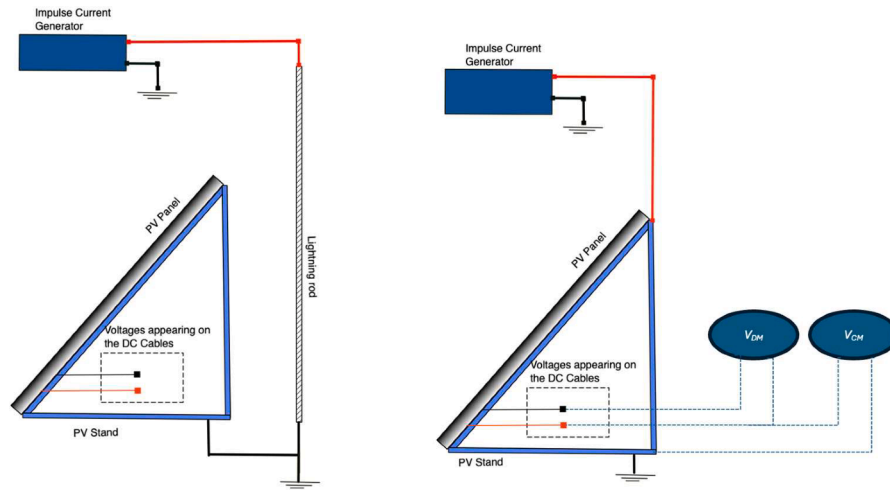


Fig. 8. 10/350 High current impulse generator.

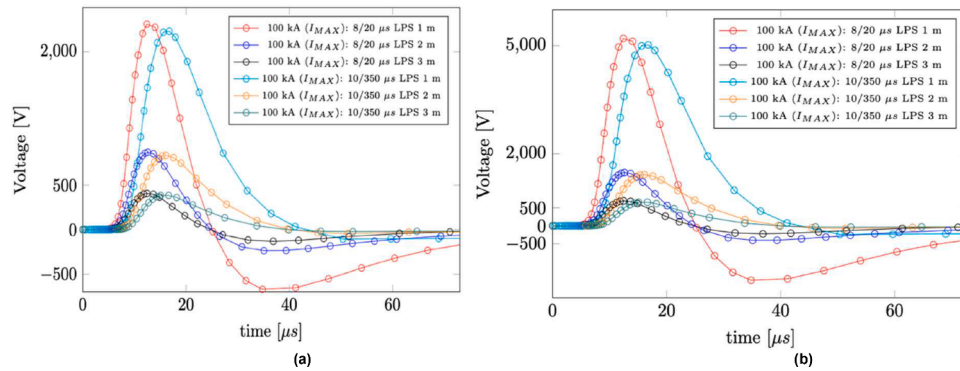


Fig. 9. Effect of changing LPS distance (a) DM (b) CM. It is easy to notice that the induced overvoltage increased with increasing distance between the LPS and the PV panel.

Table 3
Case study 1 Induced Voltages.

I_{max}	Simulation (V_{max})											
	LPS 1 metre				LPS 2 metres				LPS 3 metres			
	Differential Mode		Common Mode		Differential Mode		Common Mode		Differential Mode		Common Mode	
	8/20 μs	10/350 μs	8/20 μs	10/350 μs	8/20 μs	10/350 μs	8/20 μs	10/350 μs	8/20 μs	10/350 μs	8/20 μs	10/350 μs
5 kA	115,65 V	113,25 V	260 V	252 V	41,86 V	40,64 V	71 V	68,93 V	19,25 V	18,69 V	32,72 V	31,77 V
12,5 kA	289,12 V	280,70 V	650 V	631,07 V	104,64 V	101,59 V	177 V	171,84 V	48,11 V	47,71 V	81,79 V	79,40 V
20 kA	410 V	448,54 V	1 040 V	1.01 kV	167,42 V	162,42 V	284 V	275,72 V	76,98 V	74,73 V	130,87 V	127,05 V
100 kA	2,31 kV	2,24 kV	5.2 kV	5.04 kV	837,12 V	837,12 V	1423 V	1,38 kV	384,90 V	373,68 V	654,33 V	635,27 V

addition, this observation is critical in PV systems with microinverters, as multiple panels in an array will have separate microinverters, which will be subjected to different induced voltages depending on the distance between the external LPS and panels.

Fig. 9(b) shows the induced voltages measured in the CM configuration under impulse currents of 8/20 μs and 10/350 μs . Under extreme lightning currents (100 kA), it was observed that these voltages might exceed the minimum withstand voltage for PV inverters, as prescribed by the IEC 61,643–31:2017 [28] standard. At this impulse current magnitude, 8/20 μs impulse waveshape, the induced overvoltage measured was 5.2 kV on the DC cables. For the 10/350 μs impulse waveform, the maximum induced voltage in CM was 5.04 kV for 100 kA impulse currents. These findings are important for developing protective measures against lightning transients in microinverters.

It can be observed that the LIO maximum amplitudes differed

slightly for the 8/20 μs and 10/350 μs impulse currents. Due to the current differential, the maximum amplitudes with an 8/20 μs waveform were slightly higher than those recorded for a 10/350 μs waveform. Another difference between the induced voltage waveforms is the rise and fall times, which may affect the energy when the SPD is connected. For the 8/20 μs impulse current, the induced overvoltage waveforms had a polarity reversal caused by the quick rise and fall times and, thus, a higher peak-to-peak voltage. On the other hand, for the 10/350 μs impulse current, the induced overvoltage waveforms had a longer duration with minimal polarity reversal.

Another important issue was the voltage modes of the measurements (DM and CM configurations), as seen when comparing Fig. 9(a) and 9(b) in the 8/20 μs and 10/350 μs impulse current waveforms, respectively. Investigations have shown that the induced overvoltages across the DC cables are highly dependant on the mode of measurement, which can be

used to determine the SPD protection mode. Because induced overvoltages may appear in both DM and CM modes in PV systems, SPDs installed will be subjected to these voltages, depending on the configuration. Therefore, understanding the differences in these voltages is crucial for protection engineers when selecting an SPD protection mode. Significant differences were observed in both measurement modes, where the induced overvoltages were significantly higher in the CM configuration.

The frame of the PV panel created a geometric loop in addition to the loop created by the interconnections of the cells. Since the loop created by the loop is connected to ground, it creates a short circuit current close to the internal loop, reducing the magnetic field of the internal loop [10, 29]. Therefore, the high induced voltages in CM are owing to the high ground potential [6].

3.2. Case study 2

In the second case study, impulse current was injected into the frame of the PV panel, and the induced overvoltages on the DC cables were measured, as listed in Table 4. The highest magnitude of induced overvoltages in the DM was observed with a 100-kA injected current, where the induced overvoltages were 5.8 kV and 5.16 kV for 8/20 μ s and 10/350 μ s impulse current waveforms, respectively (Fig. 10(a)). Using injection currents of 5 kA and 12.5 kA, induced overvoltages of 275 V and 687 V were measured on the DC cables. For 20 kA, an induced overvoltage of 1.1 kV was measured. The results further confirmed the importance of a protection system for PV systems.

The induced voltages measured for the CM configuration at an impulse current of 100 kA when the impulse current is injected into the frame of the PV panel are shown in Fig 10(b). The highest induced overvoltages were 9.86 kV and 8.1 kV in 8/20 μ s and 10/350 μ s impulse waveform when a 100-kA impulse current was injected (Fig. 10(b)). When a 20-kA maximum impulse current was applied, the voltage measured was 1.82 kV. It is important to note that this case study describes a PV system without external lightning protection and represents one of the worst-case scenarios for induced overvoltages. The results further confirmed the importance of a lightning and protection system for PV systems, if not imperative.

As demonstrated, the proportional increase in the induced voltages with an impulse current signifies the risk of high lightning currents to PV panels. In this current study, for both case studies, it was schematically noticeable that the induced overvoltage increased with increasing lightning current amplitude, as illustrated in Table 4. This linearity was observed with a change in impulse current amplitude. Since the interconnection of the solar cells creates an internal loop, the induced voltage is highly influenced by the magnetic flux passing through the loop. Therefore, the magnetic flux density highly depended on the maximum current flowing through the conductor.

A comparison between Case Studies 1 and 2 indicated that the strike location significantly influences the induced overvoltages in the two case studies. In Case Study 2, when the impulse current was injected directly into the frame of the panel, the induced overvoltages were higher than those when the impulse current was injected on the LPS, a metre from the panel (Fig. 11(a) and 11(b)). It is apparent that the introduction of the LPS (in the form of a lightning rod) significantly

Table 4
Case Study 2 Induced voltages.

I_{max}	Simulation (V_{max})			
	Differential Mode		Common Mode	
	8/20 μ s	10/350 μ s	8/20 μ s	10/350 μ s
5 kA	275 V	244,75 V	466 V	404,95 V
12,5 kA	687,5 V	611,85 V	1170 V	1,01 kV
20 kA	1,1 kV	0,99 kV	1,87 kV	1,61 kV
100 kA	5,8 kV	5,16 kV	9,86 kV	8,1 kV

influenced the overvoltages. In general, variations in the magnitude of the voltages are observed by varying the location using different case studies (protection scenarios). When the waveforms were applied to the PV frame, the magnitude of the induced voltage increased owing to the stronger magnetic field interacting with the circuit, and the exposure of the lightning current was closer to the panel.

3.3. The effect of wire lengths

To investigate the influence of wire length, the length of the DC cables from the PV panel to the microinverter was increased from one metre to two and five metres. The length of the wires can affect the resistance of the circuit, because the resistance of the wire may be represented by

$$R = \rho \frac{L}{A} \quad (14)$$

where ρ , L , and A are the resistivity, length, and cross-sectional area, respectively, of the wire.

The induced overvoltages measured with a 100-kA impulse current are shown in Fig. 12(a) and (b) for case Studies 1 and 2, respectively. PV systems with microinverters usually have little DC wiring; therefore, the effect of wiring was tested with cable lengths of one, two and five metres. The maximum induced overvoltages for different cable lengths in the case studies at 100 kA are summarised in Table 5 for Case Studies 1 and 2, respectively. It can be observed that the maximum induced voltages during this investigation changed only slightly for all three cable lengths (1, 2, and 5 m). These differences were almost negligible for small cable lengths. Because the voltage drop in the cables was small, it did not affect the induced voltage across the DC cables. The results of the present study showed a slight voltage reduction owing to the increased resistance of the wires, and a slight decrease in the induced voltage was observed with increasing wire length. However, this did not result in any significant changes. In Case Studies 1 and 2, only an average of about 2 % reduction in the induced voltages was recorded at 1 m and 5 m.

3.4. Validation using experimental investigation

To validate the simulation model, the maximum induced voltages were compared to the experimental results obtained in [19] for impulse currents not exceeding 20 kA. The induced overvoltages measured in the experiments and simulations generally agree between the two studies. The results of the maximum induced voltages for the DM and CM configurations are summarised in Tables 6 and 7, respectively. Comparing the simulation predictions with experimental data showed minimal discrepancies, thereby demonstrating the accuracy of the simulation model.

Fig. 13(a) and 19 (b) compares the experimental and simulation-induced overvoltages at 20 kA for case study 1, showing their similarity.

The maximum induced voltages for the simulation results were further compared with the experimental results for each case study and using the relative error computed as follows:

$$RE(\%) = \frac{V_{sim} - V_{exp}}{V_{exp}} \quad (15)$$

Fig. 14(a) and 14(b) show the relative errors between the simulated and experimental results. The relative error did not exceed 17 % for DM and 15 % for CM-induced voltages.

3.5. Influencing factors for lightning-induced overvoltages

From our research, the results highlight various factors influencing the magnitude of induced overvoltages in PV panels. Several

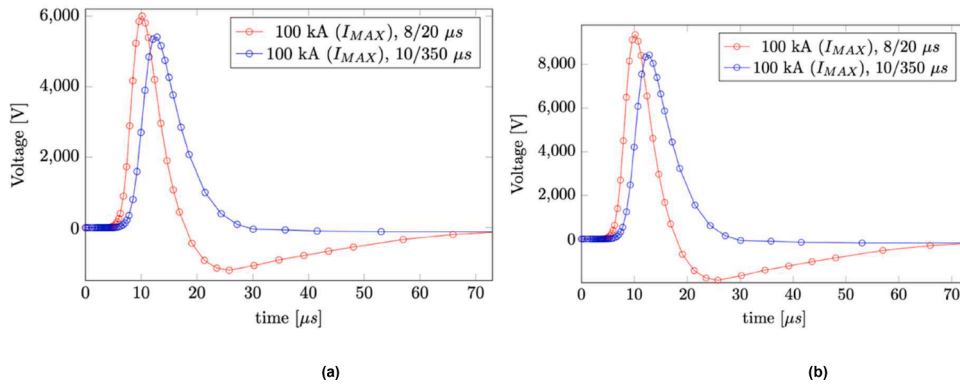


Fig. 10. Simulation Case Study 2: Induced Overvoltage (a) DM (b) CM.

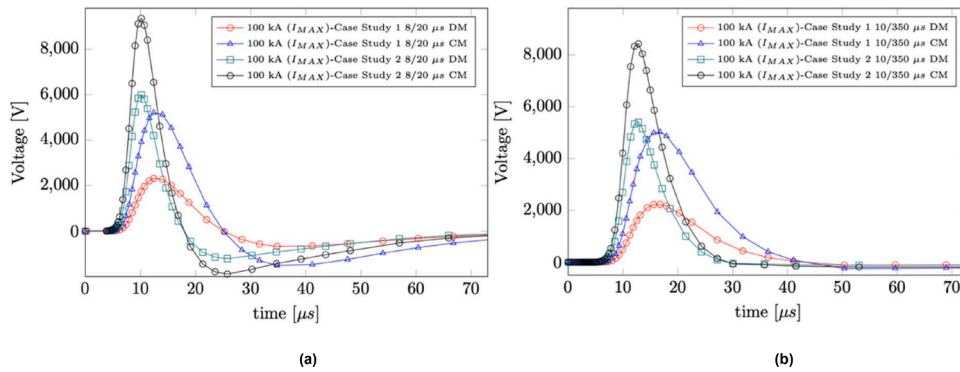


Fig. 11. The effect of mode of configuration on induced overvoltage (a) 8/20 μs (b) 10/350 μs.

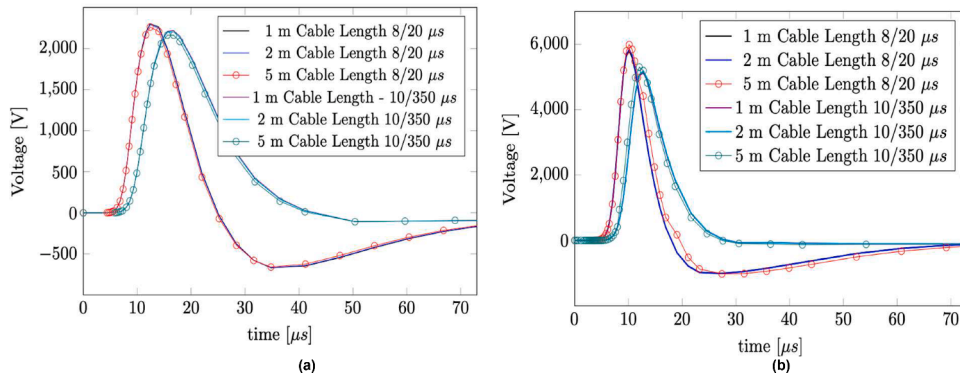


Fig. 12. Induced overvoltages with different DC cable lengths: (a) Case Study 1, (b) Case Study 2.

Table 5
Induced Voltages for different wire lengths.

I_{max}	Simulation (V_{max})			
	Case Study 1		Case Study 2	
	8/20 μs	10/350 μs	8/20 μs	10/350 μs
1 m	2302,90 V	2210,78 V	5802,90 V	5512,90V
2 m	2292,5 V	2200,60 V	5792,5 V	5502,50V
5 m	2261,40 V	2170,94 V	5711,40 V	5486,60V

parameters, such as the measurements with an LPS, the impulse current magnitude, and the location of the lightning strike, were identified as primary components [10,12,15,18,29]. The results further show that the voltage measurement scenario, performed in both DM and CM yielded different results. These voltages in a PVI can adversely affect the

connected electronic equipment, such as the microinverter. Table 8 lists the measured parameters, and their influences on the LIOs obtained from the simulations and experiments.

The results of the simulations from this study were used with selected SPD connected to the DC cables, and subsequently, the protection performance of the SPD's microinverters through energy load simulations were analysed in [30].

4. Conclusion

This study focuses on lightning-induced overvoltages in photovoltaic (PV) systems. These results show that the induced overvoltages may exceed the microinverter's impulse withstand voltage (U_w), particularly at high impulse currents and is based on the theoretical knowledge of lightning effects on electrical systems. It has been found that lightning currents flowing through LPS structures, or the PV frame can cause

Table 6
Induced Voltages DM.

I_{max}	V_{max}							
	Experiment							
	8/20 μs		10/350 μs					
	CS1	CS2	CS1	CS2	Simulation			
	CS1	CS2	CS1	CS2	CS1	CS2	CS1	CS2
5 kA	126 V	280 V	116 V	244 V	115,65 V	275 V	113,25 V	244,75 V
12,5 kA	284 V	590 V	267 V	610 V	289,12 V	687,5 V	280,70 V	611,85 V
20 kA	430 V	970 V	415 V	950 V	462 V	1,1 kV	448,54 V	0,99 kV
100 kA					2,31 kV	5,8 kV	2,24 kV	5,16 kV

Table 7
Induced Voltages CM.

I_{max}	V_{max}							
	Experiment							
	8/20 μs		10/350 μs					
	CS1	CS2	CS1	CS2	Simulation			
	CS1	CS2	CS1	CS2	CS1	CS2	CS1	CS2
5 kA	272 V	460 V	293	483 V	260 V	455 V	252 V	404,95 V
12,5 kA	660 V	992 V	732	1,16 kV	650 V	1,14 kV	631,07 V	1,01 kV
20 kA	980 V	1,71 kV	890	1,68 kV	1040 V	1.82 kV	1,01 kV	1,61 kV
100 kA					5,2 kV	9,1 kV	5,04 kV	8,1 kV

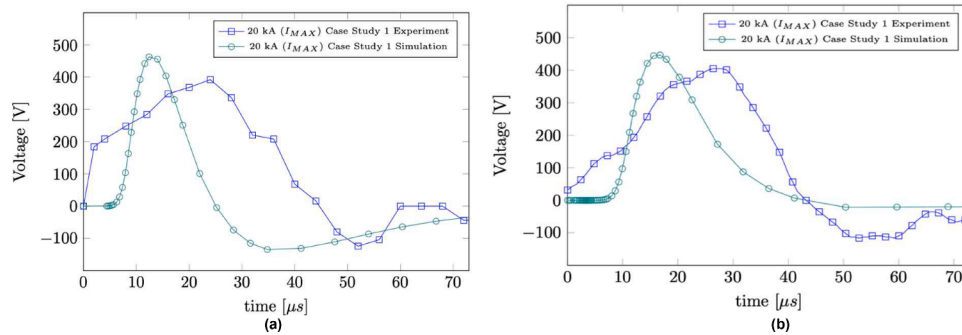


Fig. 13. Comparison of induced voltages in experiments: and simulation at 20 kA impulse current (a) 8/20 μs impulse current waveform and (b) 10/350 μs impulse current waveform.

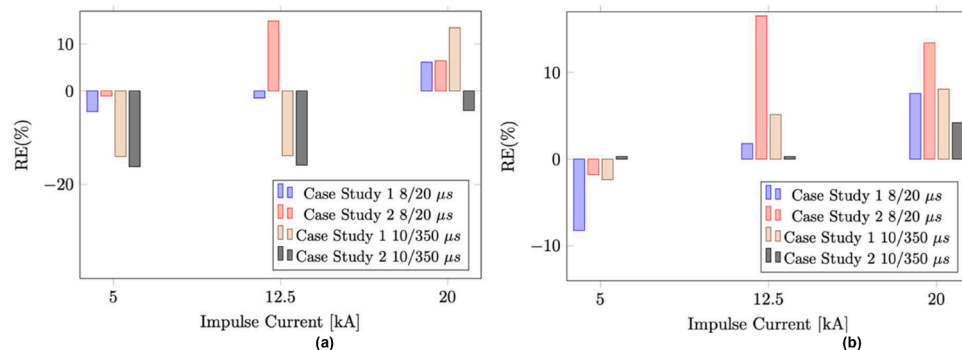


Fig. 14. The relative error between simulation and experiments. (a) DM. (b) CM.

induced overvoltages. These results can be generalised to cover different protection scenarios for PVIs with microinverters. The magnitude of these voltages varied as a function of lightning current parameters and protection cases. These parameters, including lightning current amplitude, protection scenario, mode of measurements, and circuit characteristics, indicated a variation in overvoltage magnitudes appearing on the DC cables. It was observed that the magnitude of induced overvoltages increased based on the closer strike location of the panel.

Higher magnitudes were observed in locations closer to the panel, for instance, when the lightning was injected into the frame. In addition, the distance between the LPS and the PV panel also influenced the induced overvoltages on the DC cables. Other parameters such as wire lengths on the DC cabling showed no significant effect on the induced overvoltages due to low resistances of the cables. It is also expected that, since microinverters are usually coupled to the PV panel or installed near the panel, the DC cable wire lengths would not be long and, as such, will not

Table 8
Influence factors for lightning induced voltages.

Parameter (Increase)	Lightning-Induced Overvoltage
Lightning current amplitude	A linear increase in Lightning-induced overvoltages (DM and CM) was observed when the magnitude of impulse current was increased
LPS distance	As the distance between the LPS and PV panel increased, lightning-induced overvoltages (DM and CM) decreased as a result
Lightning strike location	LIOs (DM and CM) decrease with strike distance.
Wire lengths	Had little impact on lightning-induced overvoltages (DM and CM).
Lightning current waveform	LIO maximum amplitudes differed slightly for the 8/20 μ s and 10/350 μ s impulse currents, due to the current differential.
Mode of measurements (CM and DM)	LIOs measured in CM were significantly higher than those in DM

contribute significantly to the magnitude of induced voltages. However, microinverters are sensitive electronics; it can be concluded that these induced overvoltages can exceed the microinverters' U_w . Furthermore, the induced overvoltages measured along with the recommendations can be used by protection engineers and SPD manufacturers to enhance the lightning protection of micro-inverters in PV systems.

CRedit authorship contribution statement

Simisi Mosamane: Data curation, Formal analysis, Investigation, Methodology, Project administration, Resources, Software, Validation, Visualization, Writing – original draft, Writing – review & editing.
Chandima Gomes: Supervision.

Declaration of competing interest

The authors declare that they have no known competing financial interests or personal relationships that could have appeared to influence the work reported in this paper.

Data availability

Data will be made available on request.

References

- [1] R. Hasan, S. Mekhilef, Highly efficient flyback microinverter for grid-connected rooftop PV system, *Sol. Energy* 146 (2017) 511–522.
- [2] G. Tamizhmani, Standardization and reliability testing of module-level power electronics (MLPE), in: *Proc. NREL Rel. Workshop*, 2015, pp. 1–18.
- [3] A. Vasani, L. Laskai, M. Ilic, Defining humidity test duration for microinverter reliability assessment: a physics-of-failure approach, in: *Proceedings of the 2017 IEEE Applied Power Electronics Conference and Exposition, APEC/IEEE*, 2017, pp. 2336–2340.
- [4] S. Wang, et al., Analysis of lightning-induced overvoltage waveform parameters, in: *Proceedings of the 2018 34th International Conference on Lightning Protection (ICLP)*, IEEE, 2018, pp. 1–5.
- [5] E.M. Bazelyan, Y.P. Raizer, *Lightning Physics and Lightning Protection*, CRC Press, 2000.
- [6] Y. Zhang, H. Chen, Y. Du, Lightning protection design of solar photovoltaic systems: methodology and guidelines, *Electric Power Syst. Res.* 174 (2019) 105877.
- [7] P. Chowdhuri, et al., Parameters of lightning strokes: a review, *IEEE Trans. Power Delivery* 20 (1) (2005) 346–358.
- [8] V. Cooray, "The Lightning Flash, vol. 34," Institution of Engineering and Technology (IET), Stevenage, UK, 2003.
- [9] F. Heidler, W. Zischank, Z. Flisowski, C. Bouquegneau, C. Mazzetti, Parameters of lightning current given in IEC 62305–Background, experience and outlook, in: *Proceedings of the 29th ICPL conference*, 2008.
- [10] P. Vangala, M. Ropp, K. Haggerty, K. Lynn, W. Wilson, Field measurements of lightning-induced voltage transients in PV arrays, in: *Proceedings of the 2008 33rd IEEE Photovoltaic Specialists Conference*, IEEE, 2008, pp. 1–4.
- [11] Q. Sun, et al., Three-dimensional modeling on lightning induced overvoltage for photovoltaic arrays installed on mountain, *J. Clean. Prod.* 288 (2021) 125084.
- [12] Y. Tu, C. Zhang, J. Hu, S. Wang, W. Sun, H. Li, Research on lightning overvoltages of solar arrays in a rooftop photovoltaic power system, *Electric Power Syst. Res.* 94 (2013) 10–15.
- [13] C.A. Charalambous, N.D. Kokkinos, N. Christofides, External lightning protection and grounding in large-scale photovoltaic applications, *IEEE Trans. Electromagn. Compat.* 56 (2) (2013) 427–434.
- [14] Y. Fuangfung, S. Sinthosonthishat, P. Yutthagowith, A software tool for induced voltages and currents calculation caused by lightning electromagnetic field in PV systems, in: *Proceedings of the 2015 12th International Conference on Electrical Engineering/Electronics, Computer, Telecommunications and Information Technology (ECTI-CON)*, Hua Hin, Thailand, IEEE, 2015, pp. 1–4.
- [15] N. Zaini, et al., On the effect of surge protection devices (SPDs) placement for grid-connected solar PV farm, in: *Proceedings of the 2018 34th International Conference on Lightning Protection (ICLP)*, Rzeszow, Poland, IEEE, 2018, pp. 1–5.
- [16] N.H.A. Rahim, et al., Investigation of wave propagation to PV-Solar panel due to lightning induced overvoltage, *Telkomnika* 12 (1) (2014) 47.
- [17] A. Formisano, C. Petrarca, J.C. Hernández, F.J. Muñoz-Rodríguez, Assessment of induced voltages in common and differential-mode for a PV module due to nearby lightning strikes, *IET Renew. Power Gener.* 13 (8) (2019) 1369–1378.
- [18] N.I. Ahmad, Z. Ali, M. Osman, N.H. Zaini, M.H. Roslan, Impacts of lightning-induced overvoltage on a hybrid solar PV–battery energy storage system, *Appl. Sci.* 11 (8) (2021) 3633.
- [19] S. Mosamane, C. Gomes, Lightning-Induced voltages risk for microinverters in photovoltaic installations, in: *Proceedings of the 2022 30th Southern African Universities Power Engineering Conference (SAUPEC)*, IEEE, 2022, pp. 1–6.
- [20] M. Paolone, Modeling of Lightning-Induced Voltages On Distribution Networks For the Solution of Power Quality problems, and Relevant Implementation in a Transient Program, Department of Electrical Engineering Bologna, Italy: University of Bologna, 2001, p. 117.
- [21] M. Uman, V. Rakov, G. Schnetzer, K. Rambo, D. Crawford, R. Fisher, Time derivative of the electric field 10, 14, and 30m from triggered lightning strokes, *J. Geophys. Res.: Atmos.* 105 (D12) (2000) 15577–15595.
- [22] S. Rusck, Induced Lightning Over-Voltages On Power-Transmission Lines With Special Reference to the Over-Voltage Protection of Low Voltage Networks, *Trans. Royal Institute of Technology, Stockholm*, 1958.
- [23] A.K. Agrawal, H.J. Price, S.H. Gurbaxani, Transient response of multiconductor transmission lines excited by a nonuniform electromagnetic field, *IEEE Trans. Electromagn. Compat.* (2) (1980) 119–129.
- [24] P. Chowdhuri, E.T. Gross, Voltage surges induced on overhead lines by lightning strokes, *Proc. IEE* 114 (12) (1967) 1899–1907. IET.
- [25] C. Nucci, F. Rachidi, M. Ianoz, C. Mazzetti, Comparison of two coupling models for lightning-induced overvoltage calculations, *IEEE Trans. Power Delivery* 10 (1) (1995) 330–339.
- [26] IEC, 62305-1: 2010 - Protection against Lightning: part 1: general Principles. 2010.
- [27] F. Heidler, J. Cvetic, B. Stanic, Calculation of lightning current parameters, *IEEE Trans. Power Delivery* 14 (2) (1999) 399–404.
- [28] IEC, IEC 61643-31:2018 Low-voltage surge protective devices Part 31: requirements and test methods for SPDs for photovoltaic installations. 2018.
- [29] H.J. Stern, H.C. Karner, Lightning induced EMC phenomena in photovoltaic modules, in: *Proceedings of the 1993 International Symposium on Electromagnetic Compatibility*, IEEE, 1993, pp. 442–446.
- [30] S. Mosamane, C. Gomes, Lightning-induced overvoltage protection for microinverters using surge protective devices, in: *Proceedings of the 2022 36th International Conference on Lightning Protection (ICLP)*, IEEE, 2022, pp. 138–143.